

Bursting drops

Varun Kulkarni^{1,2}, Venkata Yashasvi Lolla^{1,3}, Suhas Tamvada^{1,4}, Sushant Anand^{*1}

¹ Department of Mechanical & Industrial Engineering,
University of Illinois at Chicago, Chicago, IL 60607.

² Present Address: School of Engineering and Applied Sciences,
Wyss Institute for Biologically Inspired Engineering,
Harvard University, Cambridge, MA 02138.

³ Present Address: Department of Mechanical Engineering,
Virginia Polytechnic Institute and State University, Blacksburg, VA 24060.

⁴ Present Address: Department of Mechanical and Aerospace Engineering,
University of Florida, Gainesville, FL 32611.

* Corresponding author's e-mail address: sushant@uic.edu

Abstract

For decades, researchers worldwide have investigated phenomena related to natural/artificial oil leakages such as oil drop formation within water bodies, their rise, and oil slick evolution after they breach the water/air interface. Despite this, the event leading to slick formation—the bursting of oil drops at the liquid/air interface—has remained unnoticed thus far. In this work, we investigate this and report a counterintuitive jetting reversal that releases a daughter oil droplet inside the bulk as opposed to the upwards shooting jets observed in bursting air bubbles. We show that the daughter droplet size thus produced can be correlated to the bulk liquid properties and that its formation can be suppressed by increasing the bulk viscosity, by an overlaying layer of oil or by the addition of microparticles. We further demonstrate the significance of our results by synthesizing colloidal pickered droplets and show applications of bursting compound drops in double emulsions and studies on raindrop impact on a slick. These results could be immensely transformative for diverse areas, including climatology, oceanic/atmospheric sciences, colloidal synthesis and drug delivery.

Teaser

Drop bursting at an interface leads to a fascinating yet unreported daughter droplet production inside the bulk with tremendous consequences for several applications.

Introduction

The interaction of oil and water may be found in several diverse situations, such as emulsions for drug delivery(1-3), oil recovery(4, 5), foods(6) and oil spills(7-10) on the ocean surface. Enhancing the beneficial attributes and mitigating the deleterious effects consequently demand a detailed understanding of the underlying physical mechanisms. The merger of an oil drop with a liquid pool is therefore a model problem that can help shed light on the myriad complexities that arise in this context. In pursuit of this goal, studies so far have focused on the impact of an oil drop as it falls downwards (parallel to gravity) onto a pool liquid(9, 11-14); however, the converse, *i.e.* the rise of oil drops (due to buoyancy) from the interior of a pool of liquid and the accompanying spreading on the liquid-air interface once it has breached the surface has been relatively unexplored. As a rising droplet ruptures the intervening thin film of the bulk fluid it passes through three critical stages before finally resting on top of the bulk liquid. These are (i) the ascent of oil as a globular entity (15-17), (ii) the rupture of the thin film of the bulk liquid sandwiched between the oil droplet and air, and (iii) the spreading of the oil droplet over the surface of the bulk fluid (18). While stages (i) and (iii) have been adequately addressed, the droplet deformation occurring underneath the interface accompanying stage (ii), surprisingly received no attention despite far reaching implications.

Against this backdrop, we visualize the bursting process as a coalescence event between two liquid entities(19, 20) similar to the gentle impact of a drop on a bulk liquid. It is known that such coalescence processes proceeds in stages, partially coalescing at every stage(21, 22) leading to a cascade(9, 11, 12, 23). Strategies to modify droplet behavior during partial coalescence have also been proposed, which involve using surfactants(24) or viscoelastic fluids(25). However, these studies have been limited to oil drop impacts from above. Although applications such as oil recovery usually present situations where such coalescence events (either partial or complete) may be witnessed in rising oil droplets in an external medium, they are usually comprised of two phases and occurring at liquid-liquid interfaces(5, 22, 26). Bursting of an oil drop and its spreading on the pool of bulk liquid forming a 3-phase contact line has not been investigated so far. Consequently, several questions arise in this context: under what conditions would partial coalescence occur, are other types of coalescence scenarios possible, what is the dependence of the daughter droplet size on liquid properties, what can we glean from this understanding and how can we relate it to practical applications that until now have only been addressed for 2-phase systems?

Experiment

To address the questions outlined in the foregoing discussion, we constructed an experimental setup in which a rising oil drop gently impacts the aqueous-air interface (< 1 cm/s) as shown in the schematic in **Fig. 1a**. Although the spreading above the interface is simultaneous to the subsurface drop deformation, we focus our attention on events below the interface with the tacit assumption that the total time scale for the drop to spread far exceeds the time scale at which the oil drop deforms under the interface, and for cases where the two may be comparable, no quantitative comparisons are made for any of the deformation features. Three different oils and varying wt. % glycerine/water mixtures as bulk fluids are used. The exact composition is described in the **Methods** section of this paper. The oil droplets are chosen such that they are lighter in density (ρ_p in kg/m^3) than the bulk fluid, with a dynamic viscosity (μ_p) in the range of 0.24 to 3.005 mPa-s and with varying spreading coefficient, $S = \sigma_{pa} - \sigma_{ba} - \sigma_{pb}$ (27). Hereafter throughout the text, subscripts p and b represent parent drop and bulk phase, respectively. Here, σ_{pb} is the interfacial tension between the parent oil drop and bulk liquid (in N/m), σ_{pa} is the surface tension between the oil and air (in N/m) and σ_{ba} is the surface tension between the bulk liquid and air (in N/m). $S > 0$ represents the case when the oil has the tendency to spread on water, in contrast to the case when $S < 0$, where the oil tries to bead up. The three liquids used as the droplet phase, pentane ($S > 0$), hexadecane ($S < 0$) and silicone oil ($S > 0$), are chosen to represent this broad range of spreading coefficients. Our results are described in terms of $Oh_b = \mu_b / (\rho_b \sigma_{pb} R_p)^{1/2}$ and $\mu_r = \mu_b / \mu_p$. It is worthwhile to point out here

that the effects of gravity as defined by the Bond number, $Bo = \rho_p g R_p^2 / \sigma_{pb}$, are negligible, where g ($= 9.81$ m/s²) denotes the magnitude of gravitational acceleration pointing vertically downwards into the bulk (see **Supplementary Material Section S1** for details of experimental test conditions). It is important to note that even though we have a three-phase contact line, we resort to a description that involves just two fluids because we do not concern ourselves with the spreading or three-phase contact line motion above the interface.

Bursting of an oil drop and daughter droplet generation

Fig. 1 displays the results from different optical visualizations obtained using side view imaging. **Fig. 1b, c** shows two extreme cases of bursting, one resulting in partial coalescence and the other in complete merger or coalescence (see **Movie S1**). To comprehend the reasons behind this observation, we begin by providing a physical description of the processes involved. As the oil drop rises and the intervening thin (bulk) liquid film is ruptured (**Fig 1d**), capillary waves rapidly descend downwards, straddling the oil/water interface continuously being attenuated by the viscosity of the drop and the bulk (see **Movie S2**). If these waves do not dissipate completely when they reach the apex of the drop, they attempt to turn onto the drop, antiparallel to the direction of gravity forming a “bulge” (see **Movie S1**). On the other hand, if they dissipate completely before reaching the drop’s apex, no discernible deformation is observed as the drop integrates with the bulk.

The first of these scenarios is particularly interesting, as the bulge containing the excess energy of the interfering waves attempts to move upwards; however, its movement is inhibited by the weight and the small but finite viscosity of the drop. It can no longer continue its journey upwards and reverses direction to move parallel to gravity and against buoyancy, thereby even pulling the drop downward and ultimately pinching off leaving behind a daughter droplet. Interestingly, for negligible drop viscosities or in the case of an air bubble, this movement is exactly the opposite, leading to jetting upwards, which contrasts with our results which show jetting in the downward direction. Our observation is first of a kind for such systems comprising oil drops rupturing at an air-water interface. This downward jetting may or may not lead to the production of daughter droplets. In addition, we also observe that complete merger proceeds in stages resulting in a cascade (**Fig. 1e**, also see **Movie S3**). From a practical standpoint, it effectively shows that droplets from oil spills that rupture at the surface can leave behind residual fluid elements that may penetrate deep into the interior of the oceans and may not be simply removed by skimming the ocean surface or by dispersing the slick by adding surfactants. However, a salutary consequence of this phenomenon is its possible use in making encapsulated materials, as will be shown later in the discussion.

Prediction of regime boundaries theoretically

To probe all these aspects further, we begin by analyzing in-depth the dynamics of the waves produced upon rupture of an interface and its subsequent travel along an interface. A typical wave is depicted by the form $\xi = \xi_0 e^{\omega t + ikx}$. It is characterized by its wavelength, λ , amplitude, ξ_0 and complex frequency, ω ($= \omega_{re} + i\omega_{im}$), with t and x representing the time and spatial coordinates. When $\omega_i \neq 0$, we observe travelling waves - a case we term *jetting* and one that can result in daughter droplet production, partial coalescence, or delayed coalescence. For $\omega_{im} = 0$, we obtain standing waves that monotonically decay, a case where *jetting* is not observed, and the droplet coalesces completely. Here, ω_{re} is representative of the decay (or dissipation) rate of the waves, which, in the case of a traveling wave, is given by the first term in eqn (1) with the speed of travel given by the second term. For standing waves in comparison, we obtain two solutions for the decay rate. Furthermore, a higher amplitude, shorter wavelength and higher frequency implies higher energy, $E \sim \omega_{im}^2 \xi_0^2$ and vice versa.

With this background, we may now proceed to write the dispersion relation (28-31) between the wavenumber, k ($= 2\pi/\lambda$) and frequency or growth rate, $|\omega|$, for wave with wavelength, λ , which allows us to establish the criterion for “jetting” and “no jetting” or, alternatively, demarcate partial /delayed

coalescence from complete coalescence.

$$\omega = \underbrace{-Ak^2}_{\text{Dissipation rate, } \mathcal{D}} \pm \underbrace{\sqrt{A^2k^4 + Bk^3 - Ck}}_{\text{Wave velocity, } v = \omega/k} \quad (1)$$

In the above equation, $A = 2(\mu_b/\rho_b)(1 + \mu_r)(1 + \rho_r)^{-1}$, $B = 2\sigma_{pb}/\rho_p(1 + \rho_r)^{-1}$, $C = (\rho_r - 1)(\rho_r + 1)^{-1}$, ρ_r is the density ratio between the bulk and droplet fluid, μ_r , the viscosity ratio between the bulk and droplet fluid and other symbols are as described in the foregoing discussion. As indicated in the foregoing discussion, the term Ak^2 represents the wavelength-dependent decaying amplitude, and the frequency is given by $(A^2k^4 + Bk^3 - Ck)^{1/2}$. Of interest to us is the frequency term, which shows whether the waves will be traveling and oscillatory or standing and decaying in accordance with the sign of the term under the square root. The term Ak^2 accounts for the slowing down of the waves due to viscosity(31) of internal/external fluid which has not been considered in previous studies(11, 12, 32). This leads us to the expression for the first criticality, *i.e.*, when jetting would occur and when the waves would simply be damped by imposing the constraint that the frequency term should be less than zero. Eqn (2) gives this criticality with the constant $\varepsilon = a = 0.035$ and is represented by the black dotted line in **Fig. 2a**.

$$Oh_b < \frac{\varepsilon\mu_r}{1 + \mu_r} \quad (2)$$

Proceeding further, we establish the criterion for the second criticality, *i.e.*, when this jetting will generate drops. To achieve this, we use the fact that the waves should not have dissipated completely before reaching the bottom of the drop. Earlier studies have used this criterion but have not accounted for the slowing down of the waves owing to viscosity, which we do in our case. Mathematically, this means that we set $Dt_{apex} < 1$ (11, 12, 32), where t_{apex} is the time to reach apex and D is the dissipation rate. The length of travel for the wave is $(\pi/2)R_p$, and the velocity given by $v (= \omega/k)$ is indicated in eqn (1). These calculations yield (upon neglecting gravitational effects) an inequality like the previous criterion but with the constant $\varepsilon = b = 0.16$ and a regime boundary represented by the purple dotted line in **Fig. 2a**. In eqn (2), the constant $\varepsilon = a$ or b , where $a = 0.035$ and $b = 0.16$ (for details see **Section S2**).

To enunciate our point, we present the outlines for the different regimes at various time instances in **Fig. 2b, c and d**. The profiles in **Fig. 2c** and **Fig. 2d** do not produce drops; however, we can see a relatively sharper traveling wave at $t = 6$ ms (orange line) in comparison to the one for the standing decaying wave. This qualitatively served as a marker for distinguishing between the jetting and no jetting regimes. We also mention that although satellite drops may be produced, the criterion for satellite drops is more restrictive and enveloped by the criterion for jets producing drops. For most cases in our experiments, we did not observe any predominant satellite droplet formation. Additionally, it is noteworthy to mention that gravitational effects have been neglected and $Oh_b = (\mu_r/\sqrt{\rho_r}) Oh_p$. These results are directly related to oil spills in water bodies, which often have varying viscosities due to salinity and temperature(33).

Size of daughter droplet and scaling analysis

From the regimes identified in **Fig. 2**, we turn our attention to partial coalescence producing a daughter droplet. **Fig. 3a** schematically shows the deformed drop just before and after pinch-off. After the waves interfere at the apex, a cylindrical entity (**Fig. 3a, $t = 0$**) is formed that moves downward and is accompanied by spreading above the surface. The two effects compete against each other, leading to necking (**Fig. 3a, $t = t_1$**), which terminates with pinch off (**Fig. 3a, $t = t_{po}$**). The pressure difference during necking, Δp_{neck} , equals $\sigma_{pb}(R_1^{-1} + R_2^{-1} - 2d_{neck}^{-1})$. Since $R_1, R_2 \gg d_{neck}$, as d_{neck} tends to zero, $\Delta p_{neck} = -2d_{neck}^{-1}$ pushes the fluid outwards from the neck, ultimately leading to pinch off. Once the daughter droplet is pinched off, the volume of the daughter droplet generated ($= (4/3)\pi R_d^3$) is equal to the mass of the cylindrical entity ($= \pi d^2 l/4$) preceding its pinch off. Although satellite drops may be formed, they are noticed only for very few cases and are excluded from the scaling analysis for the sake of clarity. Furthermore, pinch off is observed only in a single stage and not in the second stage, as observed for

partial coalescence when drop impact is from above.

Fig. 3b shows the scaling for R_d/l_v with Oh_b with a power law index of -2.34 . A remarkable collapse is achieved, validating the choice of the viscous length scale $l_v = \mu_b^2/\rho_b\sigma_{pb}$ (9, 34). To derive this scaling mathematically, we treat the flow inside the deformed droplet (now in the shape of a cylinder) as inviscid(35) while that outside of it as viscous and obtain the scaling for longitudinal and radial extent, l and d . This, in conjunction with the simple mass balance as stated previously, helps us obtain the desired scaling law.

With this in mind, we balance the viscous, $F_v \sim (\mu_b V/R_p) ld$ (see **Fig. 3a**) and capillary force, $F_c \sim \sigma_{pb}d$, at the moving front of the cylindrical liquid mass. Noting that $V \sim l/T$, with T as the inertial time scale ($= (\rho_b R_p^3/\sigma_{pb})^{1/2}$), this leads us to the following result, $l/l_v \sim Oh_b^{-5/2}$. The scaling for l and d is the same, a fact confirmed by experimental data that show exponents of -2.22 and -2.25 for l and d , respectively, close to the value -2.5 (see **Section S3**). Finally, to obtain the scaling for the daughter drop radius, R_d (nondimensionalized by l_v), we use the scaling expressions for l and d in the expression conservation of mass, $4\pi R_d^3/3 \sim \pi d^2 l/4$ to yield, $R_d/l_v \sim Oh_b^{-5/2}$. The scaling exponent of -2.5 obtained here is within 7% of the experimentally obtained value of -2.34 . Despite this close agreement, it is important to note that the assumption that the flow inside the drop is inviscid while that outside is viscous may not be entirely true for all viscosity ratios, μ_r especially those where the outside fluid is of comparable viscosity to the inside fluid and is inviscid ($\mu_r \approx 1$, $Oh_b \ll 1$). Nevertheless, our scaling arguments serve to provide an estimate when these assumptions are true and show that the relative magnitudes of other effects may not be as significant for the experimental conditions we tested. The preceding discussion has described in detail the conditions under which a daughter droplet is produced and the dependence of its size on the liquid properties. In the exposition that follows, we leverage knowledge gained from this analysis in various scenarios, as represented in **Fig. 4**.

Applications: Controlling bursting cascade, synthesis of pickered drops, bursting of compound drops and relevance to drop impact studies

We develop our description here around three major themes: (i) formulating alternate methods to control daughter droplet generation, (ii) showing bursting of compound drops and its consequence in real-life applications and, (iii) demonstrating the ubiquity of bursting drops even in commonly observed drop impact (from above) on liquids.

We have shown in the preceding discussion that one of the means of controlling daughter droplet generation is by changing the bulk viscosity. Here, by impacting drops of hexadecane and silicone oil (chosen to test oils that are nonspreading, $S < 0$ and spreading, $S > 0$ in nature) at the water-air interface in succession, we create a thin film atop the water surface (**Fig. 4a**), as might usually be encountered in actual oil spills. Upon doing so, we observe that daughter droplets generated gradually diminish in size due to the gradually thickening overlaying film. The schematic alongside **Fig. 4a** shows three distinct rupture scenarios at different stages in the continuous impingement of drops. The first drop, which impacts the interface, ruptures the film of bulk liquid before spreading on top of it (squares). Upon bursting, the spreading oils completely wet the bulk liquid surface, forming a film of uniform thickness and a microscopic precursor layer(2, 9), while the nonspreading oils pseudopartially wet the surface with a macroscopic lens(9). With subsequent impacts, the drop no longer impacts a water-air interface but instead encounters a compound water-oil-air interface with a thin film of oil (circles). The volume of oil accumulated on the surface of water increases, and at a critical number of bursting events, N_i (~ 20 for spreading and ~ 30 for non-spreading oils), the compound 3-phase interface thickens to a two-phase water-oil interface (triangles), ultimately leading to daughter droplets of a constant size. In the case of spreading oils, the compound interface gradually thickens and spreads, unlike nonspreading oils, which form a thick layer quickly (at smaller N_i). This results in the formation of smaller daughter droplets for nonspreading oils compared to spreading oils, as the thick layer significantly dampens the capillary waves. Thus, via continuous impingement, droplets of constant size can be harnessed in the production

of monodispersed emulsions.

So far, we have focused only on changing liquid properties to manipulate droplet sizes. In this next effort, we introduce hydrophilic bentonite clay particles (average 15 μm diameter and in the range of 5–20 μm) in varying concentrations, ϕ from 0.5–6 wt.% into the parent drops, as shown in the schematic (**Fig. 4b**) to show a change in droplet sizes. Once the drops burst at the interface, the particles move to the oil-water interface owing to their hydrophilicity. With each bursting event (N_e), the particle coverage on the surface of the drop and at the interface increases due to the decreasing size of the drop, ultimately leading to the self-assembly of particles at the oil-water interface and preventing any further bursting events. The particles self-assemble at the surface of the drop, producing stable pickered drops, as seen in emulsions(36). As illustrated in **Fig 4b**, the initial particle concentration (ϕ) determines the number of bursting events (N_e) before a stable drop is pickered (see **Movie S4** and **Section S4**). This variation can be simply expressed by $N_e \propto 1/\phi$ (see **Movie S4** and **Section S5**). To confirm the self-assembly of particles at the oil-water interface, we performed confocal laser scanning microscopy (CLSM) on the pickered drop, labelling different components of the system with fluorophores to visualize clay particles inside the drop and found that they formed a shell (red ring) encapsulating the drop (**Fig. 4b**).

Moving to our second major focus, we explore the role of bursting in more complex systems, specifically involving compound drops. Using a coaxial nozzle, as shown in the schematics in **Fig. 4c, d**, we produce two limiting cases of *w/o* compound drops with 0.1% and 98% water-oil volume fractions. As the drops approach the water-air interface, they exhibit contrastingly different behavior (see **Movie S5**). Compound drops with a lower water volume fraction generate a compound daughter droplet with a thinner oil film surrounding it, thereby increasing the water-oil volume fraction from 0.1% to 3.4%, thus showcasing a facile mechanism for excess material removal through bursting, which has traditionally been achieved through solvent evaporation in applications such as drug delivery(37). At the other end of the spectrum, when a compound drop has a large water-oil volume fraction ($> 80\%$) and a thin surrounding oil film bursts at the water-air interface, it ruptures and fragments to produce polydispersed oil drops under the surface of water (**Fig. 4d**). The water inside the oil drop is dyed with rhodamine-B, giving it a pink color. The rupturing of an oil film inside a pool of water sheds light on a previously sparsely reported phenomenon of raindrop impact onto an oil slick. Film fragmentation shows the possibility of oil drop entrainment during rainfall over an oil spill(38). Finally, we show that bursting phenomena are prevalent even in drop impacts on liquids. To do so, we consider the impact of a silicone oil drop (dynamic viscosity ≈ 0.8 mPa-s) with a downward velocity of 0.5 m/s onto a thin film of oil covering a pool of water (**Fig. 4e**), a phenomenon commonly observed during a tanker spill. We observe that the impacting oil drop generates droplets below the water surface (shown in orange), which eventually burst and produce other daughter droplets (see **Movie S6**). Note that in drop impacts from above, droplets of such sizes are usually produced above the water surface(39) and are known primarily to entrain air bubbles(40, 41), so our demonstration is novel.

In summary, this work shows that the collapse of an oil droplet can lead to outcomes that have been previously unreported and in striking contrast to morphologies reported for partial coalescence of oil droplets gently impacting a liquid surface from above the bulk liquid/air interface. These different outcomes are outlined in a regime map based on the controlling parameters of the problem. While the principal interest of most studies until now has been oil-slick formation on the surface, the formation of droplets underneath the surface uncovered in this work suggests a new pathway by which oil contamination of oceans can proliferate, thus adversely affecting aquatic and marine life. Additionally, we show that this bursting can be, effectively controlled by introducing particles and oil films, manipulated to synthesize pickered drops used in emulsions and study raindrop impacts on oil slicks. We envision that the results presented herein have the potential to broadly impact numerous fields, including ocean/atmospheric sciences and colloidal synthesis for drug delivery/food/cosmetics, and other future applications that could emerge by creatively manipulating the phenomenon of bursting droplets.

Methods

The bulk liquids were prepared by mixing different volumes of glycerol (0 – 80 wt. % of mixture in increments of 10 wt. %) with deionized water and homogenized using a magnet stirrer. A glass chamber (30×30×20 mm³) is clamped onto an aluminum base using metal clamps and is used to hold the bulk liquids. An “L”-shaped channel inside the base connects an orifice at the center of the base to a syringe containing oil by means of a PVC tube (ID = 2 mm, length = 1210 mm; McMaster Carr). The orifice is threaded to fit nozzles of different diameters (0.7, 1.6, 2.5, 3.9 and 5.9 mm) to control the size of the oil drops generated. These nozzle diameters along with bulk liquid/droplet combinations produce droplet radii (R_p) in the range of 1.5 – 5.5 mm. The drop diameters thus obtained are below the capillary length ($l_c = (\sigma_{pb}/\Delta\rho g)^{1/2}$) corresponding to a Bond number, $Bo (= \Delta\rho g R_p^2 \lesssim 1)$. The oil drops were generated using a syringe pump with a constant flow rate of 0.5 ml/min. A high-speed camera (Photron Mini AX) was attached to InfiniProbe with an SFX-2 objective and SL mount to record the side view of the bursting events at 5000 fps. with a pixel resolution of 840×2400, which gave a spatial resolution of 2 μ m.

References and notes

1. L. Y. Chu, Utada, A. S., Shah, R. K., J. W. Kim, Weitz, D. A., Controllable monodisperse multiple emulsions. *Angew. Chem* **46**, 8970-8974 (2007).
2. J. Feng, Nanoemulsions obtained via bubble-bursting at a compound interface. *Nat. Phys.* **10**, 606-612 (2014).
3. I. F. Guha, S. Anand, K. K. Varanasi, Creating nanoscale emulsions using condensation. *Nat. Commun* **8**, 1371-1371 (2017).
4. L. Wang, Advances in improved/enhanced oil recovery technologies for tight and shale reservoirs. *Fuel* **210**, 425-445 (2017).
5. L. L. Schramm, *Emulsions, foams, and suspensions: fundamentals and applications*. (John Wiley & Sons, 2006).
6. E. Dickinson, Food emulsions and foams: Stabilization by particles. *Curr. Opin. Colloid Interface Sci* **15**, 40-49 (2010).
7. J. Beyer, H. C. Trannum, T. Bakke, P. V. Hodson, T. K. Collier, Environmental effects of the Deepwater Horizon oil spill: A review. *Mar. Pollut. Bull* **110**, 28-51 (2016).
8. A. Jernelöv, How to defend against future oil spills. *Nature* **466**, 182-182 (2010).
9. V. Kulkarni, V. Y. Lolla, S. R. Tamvada, N. Shirdade, S. Anand, Coalescence and spreading of drops on liquid pools. *J. Colloid Interface Sci* **586**, 257-268 (2021).
10. C. H. Peterson, Long-term ecosystem response to the Exxon Valdez oil spill. *Science* **302**, 2082-2086 (2003).
11. F. Blanchette, T. P. Bigioni, Partial coalescence of drops at liquid interfaces. *Nat. Phys.* **2**, 254-254 (2006).
12. F. Blanchette, T. P. Bigioni, Dynamics of drop coalescence at fluid interfaces. *J. Fluid Mech* **620**, 333-352 (2009).
13. U. Jain, M. Jalaal, D. Lohse, D. van der Meer, Deep pool water-impacts of viscous oil droplets. *Soft Matter* **15**, 4629-4638 (2019).
14. H. Lhuissier, C. Sun, A. Prosperetti, D. Lohse, Drop fragmentation at impact onto a bath of an immiscible liquid. *Phys Rev Lett* **110**, 264503 (2013).
15. N. Abi Chebel, J. Vejražka, O. Masbernat, F. Risso, Shape oscillations of an oil drop rising in water: effect of surface contamination. *J. Fluid Mech* **702**, 533-542 (2012).
16. M. Ohta, Akama, Y., Yoshida, Y., Sussman, M., Influence of the viscosity ratio on drop dynamics and breakup for a drop rising in an immiscible low-viscosity liquid. *J. Fluid Mech* **752**, 383-409 (2014).
17. I. U. Vakarelski, Yang, F., Tian, Y. S., Li, E. Q., Chan, D. Y., Thoroddsen, S. T. , Mobile-surface bubbles and droplets coalesce faster but bounce stronger. *Sci. Adv* **5**, eaaw4292 (2019).
18. D. W. Camp, The spreading of oil on water in the surface-tension regime. *J. Fluid Mech* **184**, 445-462 (1997).
19. C. R. Anthony, M. T. Harris, O. A. Basaran, Initial regime of drop coalescence. *Phys. Rev Fluids* **5**, (2020).
20. J. D. Paulsen, , Justin C. Burton, Sidney R. Nagel, Santosh Appathurai, Michael T. Harris, Osman A. Basaran, The inexorable resistance of inertia determines the initial regime of drop coalescence. *Proc. Natl. Acad. Sci. U.S.A* **109**, 6857-6861 (2012).
21. H. P. Kavehpour, Coalescence of drops. *Annu. Rev. Fluid Mech* **47**, 245-268 (2015).

22. G. E. Charles, S. G. Mason, The mechanism of partial coalescence of liquid drops at liquid/liquid interfaces. *J. Colloid Sci* **15**, 105-122 (1960).
23. T. Gilet, K. Mulleners, J. P. Lecomte, N. Vandewalle, S. Dorbolo, Critical parameters for the partial coalescence of a droplet. *Phys. Rev. E* **75**, 36303-36303 (2007).
24. S. Shim, H. A. Stone, Damped coalescence cascade of liquid drops. *Phys. Rev. Fluids* **2**, 44001-44001 (2017).
25. X. Chen, Mandre, S., Feng, J. J., An experimental study of the coalescence between a drop and an interface in Newtonian and polymeric liquids. *Phys. Fluids* **18**, 92103-92103 (2006).
26. Z. Mohamed-Kassim, E. K. Longmire, Drop coalescence through a liquid/liquid interface. *Phys. Fluids* **16**, 2170-2181 (2004).
27. P. G. De Gennes, F. Brochard-Wyart, D. Quéré, *Capillarity and wetting phenomena: drops, bubbles, pearls, waves*. (Springer Science & Business Media, 2004).
28. T. Funada, D. Joseph, Viscous potential flow analysis of Kelvin-Helmholtz instability in a channel. *J. Fluid Mech* **445**, 263-283 (2001).
29. D. D. Joseph, J. Wang, The dissipation approximation and viscous potential flow. *J. Fluid Mech* **505**, 365-377 (2004).
30. H. Kim, J. Padrino, D. Joseph, Viscous effects on Kelvin-Helmholtz instability in a channel. *J. Fluid Mech* **680**, 398-416 (2011).
31. J. C. Padrino, D. D. Joseph, Correction of Lamb's dissipation calculation for the effects of viscosity on capillary-gravity waves. *Phys. Fluids* **19**, 82105-82105 (2007).
32. J. S. Lee, Weon, B.M., Park, S.J., Je, J.H., Fezzaa, K. and Lee, W.K., Size limits the formation of liquid jets during bubble bursting. *Nat. Commun* **2**, 1-7 (2011).
33. M. Jochum, G. Danabasoglu, M. Holland, Y. O. Kwon, W. G. Large, Ocean viscosity and climate. *J. Geophys. Res* **113**, (2008).
34. A. M. Gañán-Calvo, Revision of bubble bursting: Universal scaling laws of top jet drop size and speed. *Phys. Rev. Lett* **119**, 204502 (2017).
35. R. F. Day, E. J. Hinch, J. R. Lister, Self-similar capillary pinchoff of an inviscid fluid. *Phys. Rev. Lett* **80**, 704-704 (1998).
36. B. P. Binks, Lumsdon, S.O., Pickering emulsions stabilized by monodisperse latex particles: effects of particle size. *Langmuir* **17**, 4540-4547 (2001).
37. T. Sheth, S. Seshadri, T. Prileszky, M. E. Helgeson, Multiple nanoemulsions. *Nat. Rev. Mater* **5**, 214-228 (2020).
38. D. W. Murphy, Li, C., d'Albignac, V., Morra, D., Katz, J., Splash behaviour and oily marine aerosol production by raindrops impacting oil slicks. *J. Fluid Mech* **780**, 536-577 (2015).
39. A. M. Worthington, R. S. V. Cole, Impact with a liquid surface, studied by the aid of instantaneous photography. *Philos. Trans. Royal Soc. A* **189**, 137-148 (1897).
40. M. H. W. Hendrix, W. Bouwhuis, D. van der Meer, D. Lohse, J. H. Snoeijer, Universal mechanism for air entrainment during liquid impact. *Journal of Fluid Mechanics* **789**, 708-725 (2016).
41. T. Tran, H. de Maleprade, C. Sun, D. Lohse, Air entrainment during impact of droplets on liquid surfaces. *J. Fluid Mech* **726**, (2013).
42. J. B. Segur, and Helen E. Oberstar, Viscosity of glycerol and its aqueous solutions. *Ind. Eng. Chem. Res* **43**, 2117-2120 (1951).
43. C. L. Yaws, *Yaws' Handbook of Physical Properties for Hydrocarbons and Chemicals*. (Elsevier, 2015).
44. M. K. Awasthi, R. Asthana, G. S. Agrawal, Pressure corrections for the potential flow analysis of Kelvin-Helmholtz instability with heat and mass transfer. *International Journal of Heat and Mass Transfer* **55**, 2345-2352 (2012).
45. A. Prosperetti, Motion of two superposed viscous fluids. *Phys. Fluids* **24**, 1217-1223 (1981).
46. H. Lamb, *Hydrodynamics*. (University Press, 1924).
47. L. D. Landau, Evgenii Mikhailovich Lifshitz, *Fluid Mechanics: Course of Theoretical Physics*. (Elsevier, 2013), vol. 6.
48. S. Krishnan, E. J. Hopfinger, Baburaj A. Puthenveetil, On the scaling of jetting from bubble collapse at a liquid surface. *Journal of Fluid Mechanics* **822**, 791-812 (2017).
49. J. R. Lister, H. A. Stone, Capillary breakup of a viscous thread surrounded by another viscous fluid. *Physics of Fluids* **10**, 2758-2764 (1998).

50. K. Golemanov, S. Tcholakova, P. A. Kralchevsky, K. P. Ananthapadmanabhan, A. Lips., Latex-Particle-Stabilized Emulsions of Anti-Bancroft Type. *Langmuir* **22**, 4968-4977 (2006).

Acknowledgments

The authors thank Navid Saneie for SEM images of the bentonite clay particles.

Funding: Society in Science, Branco Weiss fellowship (SA)
National Science Foundation EAGER grant no. 2028571 (SA)
UIC College of Engineering (SA)

Author Contributions

Conceptualization: SA

Methodology: VK, SA

Validation: VK

Formal analysis: VK

Investigation: VYL, ST, VK

Resources: SA

Data curation: VYL, VK, ST

Writing-original draft: VK

Writing – Reviewing & editing: VK, ST, SA

Visualization: VK, SA

Supervision: SA

Project Administration: SA

Funding acquisition: SA

Competing Interests: The authors declare that they have no competing interests.

Data and materials availability: All data required to evaluate the conclusions in the paper are present in the paper and/or Supplementary materials.

Additional information

Extended data is available for this paper at <https://doi.org/xxx>.

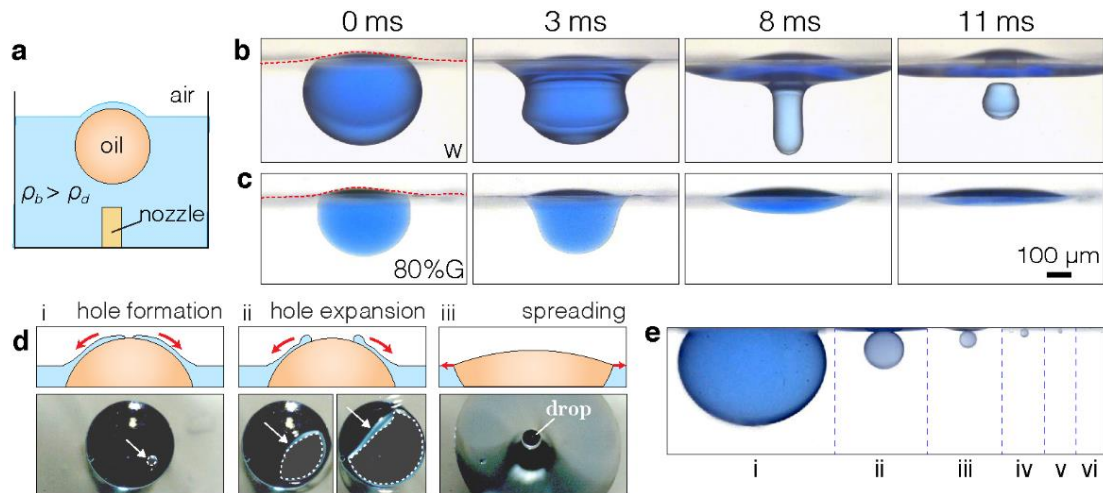


Figure 1 | Mechanism and outcomes of a liquid bursting an oil drop. **a.** The schematic shows the experimental setup used to gently impact oil drops at a liquid-air interface. A nozzle is used to generate droplets of uniform size. **b.** and **c.** show the changing morphology of a Hexadecane drop during bursting at different time instants as indicated above. $t = 0$ is considered just before the rupture of the film of bulk liquid. **b.** represents a bulk liquid low viscosity (water), leading to the generation of a secondary daughter droplet. **c.** shows the time evolution of the drop when introduced in a liquid with high viscosity (20 wt. % water + 80 wt. % glycerol), leading to complete emergence without the formation of a downward jet. **d.** The schematic and top view of the different stages of bursting and spreading. The white dashed lines show the liquid film during the three stages of bursting - (i) hole formation, (ii) hole expansion, and (iii) spreading of the drop. **d.** (iii) also shows the daughter droplet below the surface of the bulk liquid. **e.** The generation of a daughter droplet resets the system to the initial scenario with a drop at the liquid-air interface. A cascade of further bursting events leads to the generation of subsequent daughter droplets before complete emergence of the oil drop.

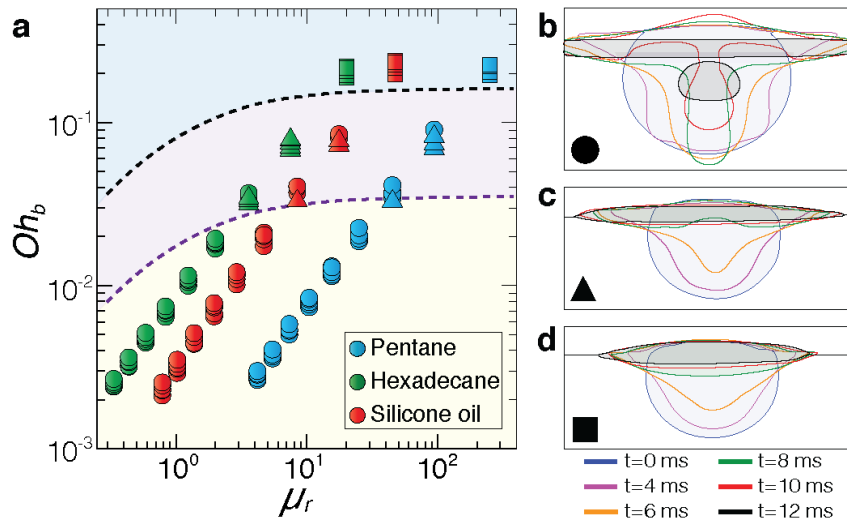


Figure 2 | Phase diagram of the outcome and corresponding contours of drops during bursting.

a. The three different regimes, jetting with daughter droplet generation (filled circles), jetting (filled triangles) and no-jetting (filled squares) observed depending on the viscosity ratio (μ_r) and the Ohnesorge number of the bulk (Oh_b). Dotted purple line shows the first transition boundary (criticality) from jetting with daughter droplet generation to only jetting. Dotted black line shows the second transition boundary (criticality) from only jetting to no-jetting. At lowest Oh_b and μ_r (circles) **b.** a downward jet leading to the generation of a daughter droplet is observed. At moderate Oh_b and μ_r (triangles) **c.** capillary waves are found to deform the drop to produce a downward jet, however, they are not strong enough to generate a secondary drop. At highest Oh_b and μ_r (squares) **d.** the capillary waves are significantly damped due to viscosity and no jet is observed. **b - d,** show the profiles of the drop in the three regimes at different time instances as indicated.

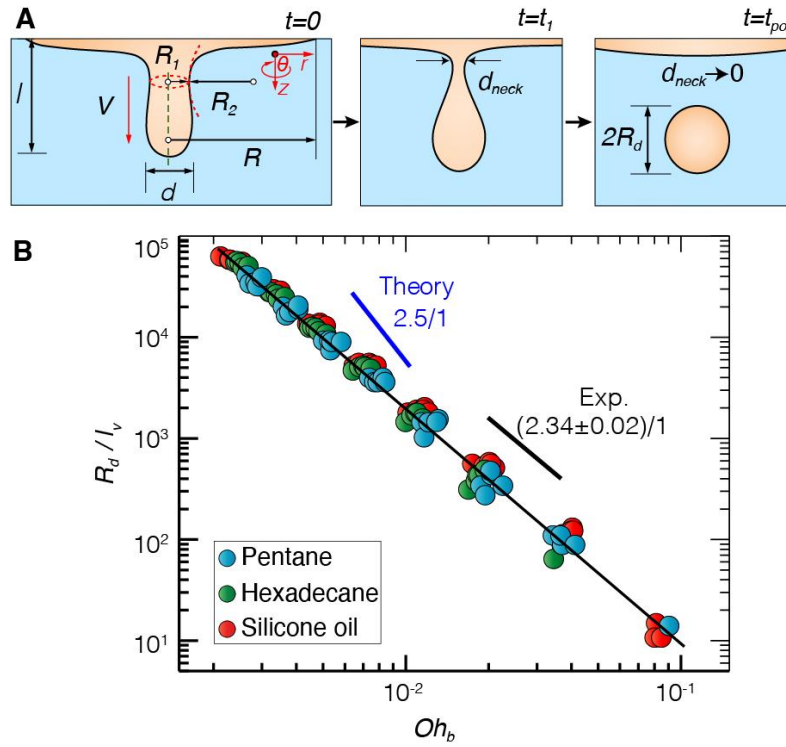


Figure 3 | Mechanism of generation of daughter droplet and its scaling with bulk liquid properties. **a**, Schematic shows the profile of the drop at three instances of time, t_0 , the time when the capillary wave deforms the drop to form a cylindrical entity, t_1 , the time when pinch off begins, and t_{po} , the time at which a daughter droplet is pinched off. The volume of the cylinder formed by the downward jet just before pinch-off equals the volume of the daughter droplet. The theoretical scaling obtained through the equivalence of the volumes of the cylinder and daughter droplet and its comparison with experimental data. **b**, Scaling for the radius of the daughter droplet, R_d (non-dimensionalized using the inertia-visco-capillary length scale) with the bulk Ohnesorge number, Oh_b . The experimental scaling exponent ($R_d/l_v \sim Oh_b^{-2.34 \pm 0.02}$) is found to be -2.34 as compared to the one by force balance which gives a value of -2.50 .

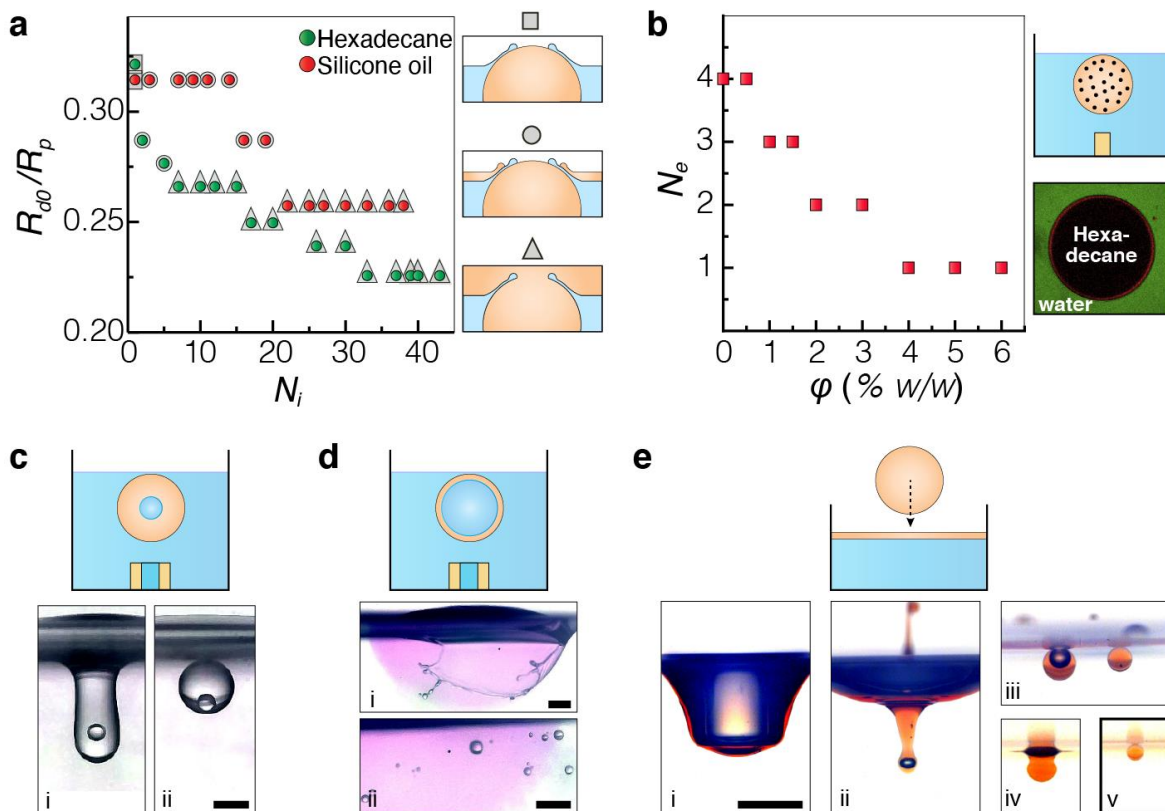


Fig. 4 | Broader aspects of bursting at liquid-air interface. **a.** Evolution of the daughter droplet radius to the parent drop radius upon successive impacts for non-spreading (hexadecane) and spreading (silicone oil) oil droplets from below. The schematic shows the various scenarios corresponding to the symbols in the plot. **b.** The maximum number of bursting events before the cascade arrest as a function of particle concentration (ϕ) within the oil drop (as shown in the schematic). Also shown is an image of a Hexadecane drop with self-assembled clay particles (red ring) at oil-water interface captured using CLSM after the first bursting event (bulk water – green, oil – black). **c. & d.** schematics show the extreme cases (of water-oil volume ratio) of a compound drop introduced at the water-air interface. **c.** shows the outcome of bursting of a compound drop with low water-oil volume ratio. **d.** shows the bursting outcome in form of the oil film fragmentation inside bulk water at very high water-oil volume ratio in the parent drop. **e.** Schematic shows the impact of an oil (Hexadecane) drop onto a pool of water covered by a thin layer of oil ($\gg 30$ nm). Accompanying figures show the entrainment of oil drops (**e(i)** – **e(iii)**) upon impact of the drop (downward velocity 0.5 m/s). The entrained drops burst (**e(iv)**) and produce a daughter droplet (**e(v)**).

Supplementary materials

Section S1. Experimental test conditions

Section S2. Wave propagation after bursting of an oil drop

Section S3. Scaling for diameter of daughter droplets, D_d

Section S4. Synthesis of pickered drops

Section S5. Partial coalescence: Daughter droplet cascade

Fig. S1. Wave propagation on drop interface.

Fig. S2. Criterion for jetting.

Fig. S3. Pinch off mechanism.

Fig. S4. Scaling of cylinder during pinch off.

Fig. S5. Daughter droplet size.

Fig. S6. SEM of Bentonite particles.

Fig. S7. Mechanism of Pickered drop synthesis.

Fig. S8. Adsorption of bentonite particles.

Table S1. Interfacial properties of oil drops and bulk liquids.

Table S2. Non-dimensional liquid properties of Hexadecane.

Table S3. Non-dimensional liquid properties of Silicone oil.

Table S4. Non-dimensional liquid properties of Pentane.

Table S5. Description of non-dimensional quantities.

Table S6. Dimensional scales used in this study.

Movie S1. Drop bursting events in different bulk liquids.

Movie S2. Rupture of bulk liquid film.

Movie S3. Cascade of daughter droplet generation events.

Movie S3. Effect of particle concentration on arrest of daughter droplet cascade,

Supplementary Material References (28, 29, 31, 35, 42-50)

Correspondence & requests for materials should be addressed to SA at sushant@uic.edu

Supplementary Material

Bursting drops

Varun Kulkarni, Venkata Yashasvi Lolla, Suhas Rao Tamvada, Sushant Anand

Corresponding author. Email: sushant@uic.edu

This PDF file includes:

S1 Experimental test conditions

S2 Wave propagation after bursting of an oil drop

S2.1 Criterion for jetting - the first criticality

S2.2 Criterion for jetting producing daughter droplets - the second criticality

S3 Scaling for radius of daughter droplets, R_d

S3.1 Scaling for ' l ' and ' d '

S4 Synthesis of pickered drops

S5 Partial Coalescence: Daughter droplet cascade

S5.1 Number of daughter droplet generation events, N_e before complete coalescence

S5.2 Arrest of partial coalescence with clay particles, N_e as function of ϕ

S6 Supplementary Movies

S1. Experimental test conditions

In Table S1 we provide the properties of the oils tested in this work (hexadecane, pentane, 1.5 cSt silicone oil), and the range of drop sizes for the tested oils when in contact with bulk glycerine-water solutions (by weight). The values for dynamic viscosity (μ) for aqueous solutions of glycerol and oils were taken from literature (42, 43) and Sigma Aldrich[®]. The surface tension values (σ) of oils, aqueous glycerol solutions, and the interfacial tension values between glycerol-water solution and various oils were measured using a goniometer (OCA 15Pro, Dataphysics GmbH, Germany) at ambient conditions (23°C, 20% RH). The surface tension of oils (σ_{pa}) - hexadecane, pentane and silicone oil was measured as 19 mN/m, 15.9 mN/m and 27 mN/m respectively, where subscript ‘p’ represents parent drop and ‘a’, air. From these measurements, the spreading coefficient of oil on water (S_{pb}) was calculated as $S_{pb} = \sigma_{pa} - \sigma_{ba} - \sigma_{pb}$ where subscript ‘b’ represents bulk. Properties of air, $\mu_a = 0.89 \text{ mPa} \cdot \text{s}$ and $\rho_a = 1.225 \text{ kg/m}^3$ are taken at the same ambient conditions as above.

Table S1: Interfacial tension (σ_{pb} in mN/m), Spreading coefficient, (S_{pb} in mN/m) and Parent drop diameter ($D_p = 2R_p$ in mm). In air, the range of drop diameters for hexadecane were 1.54 to 2.11 mm, silicone oil 1.493 to 2.092 mm and pentane 1.333 to 1.832 mm.

Liquid	Air	Hexadecane			Silicone Oil			Pentane		
	σ_{pa}	σ_{pb}	S_{pb}	D_p	σ_{pb}	S_{pb}	D_p	σ_{pb}	S_{pb}	D_p
Water	71.9	52.1	- 7.2	5.5 to 6.8	44.1	8.7	7.0 to 10.1	48.1	7.1	4.7 to 6.0
10% Glycerol	71.2	49.7	- 5.5	5.2 to 6.8	42.8	9.4	6.4 to 9.2	44.5	10.8	4.6 to 5.9
20% Glycerol	70.6	45.8	- 2.2	4.9 to 6.4	37.9	13.7	6.0 to 8.1	41.1	13.6	4.2 to 5.7
30% Glycerol	69.8	42.8	- 0.04	4.8 to 6.4	34.3	16.5	5.6 to 8.1	39.1	14.8	4.2 to 5.5
40% Glycerol	69.1	40.5	1.6	4.5 to 6.0	32.8	17.3	5.3 to 7.4	36.3	16.9	4.0 to 5.3
50% Glycerol	68.2	37.3	3.9	4.4 to 5.7	28.9	20.3	5.0 to 7.3	35.0	17.3	3.6 to 5.2
60% Glycerol	67.5	35.2	5.3	4.1 to 5.6	26.2	22.3	4.7 to 7.0	35.7	15.9	3.3 to 5.2
70% Glycerol	66.7	32.6	7.1	4.1 to 5.5	25.5	22.2	4.7 to 6.4	33.2	17.0	3.1 to 5.4
80% Glycerol	65.8	29.9	8.9	3.8 to 5.3	24.2	22.6	4.3 to 6.3	31.1	18.8	3.8 to 5.1

Based on Table S1, we calculated non-dimensional parameters namely, viscosity ratio, $\mu_r (= \mu_b/\mu_p)$, density ratio, $\rho_r (= \rho_b/\rho_d)$, Ohnesorge number, $Oh_b (= \mu_b/\sqrt{\sigma_{pb}\rho_b R_p})$, Bond number, $Bo (= \Delta\rho g R_p^2/\sigma_{pb})$ and $\Delta\rho = \rho_b - \rho_p$. Here, R_p is the radius of the parent drop and D_p is the diameter of the parent drop ($= 2R_p$) expressed in m. The corresponding values of these numbers are given in Tables S2,S3,S4.

Table S2: Table of Oh , Bo , Density ratio, ρ_r and viscosity ratio, μ_r for Hexadecane.

Drop	Bulk liquid	ρ_r	μ_r	$Oh \times 10^{-3}$	Bo
Hexadecane	Air	1.6×10^{-3}	6.0×10^{-3}	20.2 to 23.7	0.16 to 0.31
	Water	1.3	0.33	2.4 to 2.7	0.33 to 0.51
	10% Glycerol	1.33	0.44	3.2 to 3.6	0.34 to 0.51
	20% Glycerol	1.36	0.59	4.5 to 5.1	0.35 to 0.61
	30% Glycerol	1.39	0.83	6.4 to 7.5	0.38 to 0.69
	40% Glycerol	1.43	1.24	10.0 to 11.5	0.39 to 0.69
	50% Glycerol	1.46	2.00	16.9 to 19.4	0.43 to 0.74
	60% Glycerol	1.50	3.59	31.6 to 36.9	0.45 to 0.83
	70% Glycerol	1.53	7.49	67.7 to 78.8	0.49 to 0.89
	80% Glycerol	1.57	20.00	188.1 to 220.8	0.49 to 0.94

Table S3: Table of Oh , Bo , Density ratio, ρ_r and viscosity ratio, μ_r for Silicone Oil.

Drop	Bulk liquid	ρ_r	μ_r	$Oh \times 10^{-3}$	Bo
Silicone Oil	Air	1.44×10^{-3}	0.014	10.5 to 12.3	0.19 to 0.37
	Water	1.17	0.79	2.1 to 2.5	0.41 to 0.84
	10% Glycerol	1.20	1.02	2.9 to 3.5	0.39 to 0.83
	20% Glycerol	1.23	1.38	4.4 to 5.1	0.44 to 0.83
	30% Glycerol	1.26	1.95	6.5 to 7.8	0.49 to 1.03
	40% Glycerol	1.29	2.91	10.2 to 12.1	0.51 to 1.02
	50% Glycerol	1.32	4.69	17.5 to 20.4	0.58 to 1.22
	60% Glycerol	1.35	8.44	33.2 to 40.6	0.62 to 1.39
	70% Glycerol	1.38	17.60	72.7 to 84.9	0.69 to 1.28
	80% Glycerol	1.42	47.00	197.3 to 234.0	0.66 to 1.45

Table S4: Table of Oh , Bo , Density ratio, ρ_r and viscosity ratio, μ_r for Pentane.

Drop	Bulk liquid	ρ_r	μ_r	$Oh \times 10^{-3}$	Bo
Pentane	Air	1.95×10^{-3}	0.075	10.5 to 12.3	0.21 to 0.42
	Water	1.6	4.19	2.6 to 2.9	0.42 to 0.69
	10% Glycerol	1.63	5.460	3.5 to 4.0	0.46 to 0.76
	20% Glycerol	1.67	7.330	5.0 to 5.8	0.45 to 0.82
	30% Glycerol	1.71	10.40	7.3 to 8.4	0.50 to 0.84
	40% Glycerol	1.76	15.50	11.4 to 13.1	0.52 to 0.90
	50% Glycerol	1.8	25.00	18.7 to 22.5	0.45 to 0.95
	60% Glycerol	1.84	45.00	32.9 to 41.2	0.40 to 0.98
	70% Glycerol	1.88	93.80	69.1 to 90.5	0.41 to 1.20
	80% Glycerol	1.93	250.00	194.3 to 225.8	0.65 to 1.19

S2. Wave propagation after bursting of an oil drop

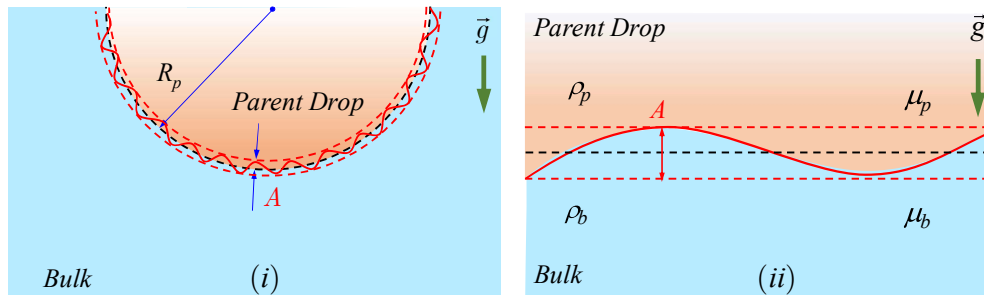


Figure S1: Schematic showing (i) capillary waves at the interface of the parent drop, and (ii) a zoomed-in view of the oil/bulk liquid interface approximating it to a plane since $A \ll D$ where A is twice the amplitude of the disturbance.

We begin by utilizing an expression analogous to the dispersion relation (eqn (1)) for two superposed fluids in the long wave limit as outlined in previous works (28, 45) and corrected for viscous pressure (31, 29, 44). The pressure

correction to the analysis is required to account for the irrotational pressure due to the vorticity layer (29, 44). The schematic of the situation is shown in Figure S1. The small amplitude of the wave (A) in comparison to the the parent drop diameter $D_p (= 2R_p)$ warrants the use of instability analysis for a flat interface.

$$\omega = \underbrace{-2k^2 \left(\frac{\mu_p + \mu_b}{\rho_p + \rho_b} \right)}_{\text{Rate of viscous dissipation/decay } \mathcal{D}} \pm \underbrace{\sqrt{4k^4 \left(\frac{\mu_p + \mu_b}{\rho_p + \rho_b} \right)^2 - \frac{\sigma k^3 + (\rho_b - \rho_p) g k}{\rho_b + \rho_p}}}_{\text{Time scale, } \tau_{\text{wave}} = 1/\omega \implies \text{Wave speed, } v = \frac{\omega}{k}} \quad (1)$$

The two terms in the underbrace above are representative of the rate of viscous decay/dissipation and specifically the velocity of the traveling waves (v). We use the dispersion relation (eqn (1)) in the long wave approximation which implies a smaller value of wavenumber, $k (= 2\pi/\lambda)$ and high viscosity ratio between the bulk (b) and the parent drop (p) liquid. Conversely, for low viscosity ratios, the instability is pushed to shorter wavelengths implying a large value of k and smaller value of wavelength, λ . This is reflected particularly in the dissipation term, \mathcal{D} in equation (eqn (1)) which differs by a factor of two depending on whether we are in short or the long wavelength limit (46, 47). For further exposition we use the dispersion relation in the long wavelength limit with the tacit assumption that for intermediate wavelengths (and by extension for intermediate viscosity ratios) the difference may be reflected by the constant prefactor to the expression in the long wavelength approximation which exists in the open interval between 0 and 1.

Additionally, it is worthwhile to note that the term in the underbrace which describes the dissipation rate, \mathcal{D} may be compared to the expression in the case when the parent drop (p) phase is inviscid (*e.g.* air). For such a scenario, we expect the expression given in (eqn (1)) to converge to the one available in literature (46, 47). Setting $\mu_p = 0$ and $\rho_p = 0$ we recover the dissipation rate of $2\mu_b k^2 / \rho_b$ for an inviscid fluid superposed above a viscous fluid with dynamic viscosity μ_b and density ρ_b . The second term in the underbrace in (eqn (1)) representing the wave velocity is corrected for the slowing down due to viscosity (of both fluids) and is given by the term, $4k^4 \left(\frac{\mu_p + \mu_b}{\rho_p + \rho_b} \right)^2$.

Continuing further we recast (eqn (1)) in terms of non-dimensional quantities for which we define the following,

$$\alpha = kR_p, \quad \beta = \omega\tau, \quad \mu_r = \frac{\mu_b}{\mu_p}, \quad \rho_r = \frac{\rho_b}{\rho_p} \quad (2)$$

Here, α is the non-dimensional wave number scaled by the parent drop radius, R (in m), β is the non-dimensional growth rate scaled by the characteristic time scale, τ (in s), σ_{pb} is the interfacial tension between the bulk fluid and the parent drop (in mN/m), μ is the dynamic viscosity (in $Pa-s$), g is the acceleration due to gravity (in m^2/s) and V is the characteristic velocity scale (in m/s) as shown in Figure S1. Before writing equation (1) in non-dimensional terms we need to identify the dimensionless groups of the problem. Using the scales identified (2) we define the following non-dimensional groups and list them in table S5 below.

It is pertinent to note that Oh_p and Oh_b *i.e.* the parent drop and bulk Ohnesorge numbers are related to each other by the following expression,

$$Oh_p = \frac{\sqrt{\rho_r}}{\mu_r} Oh_b \quad (3)$$

Furthermore for our study the bulk phase comprised of water and glycerine-water mixtures while the parent drop phase comprised of hexadecane, silicone oil and pentane respectively. Making substitutions for the scales identified in eqn (2) and the dimensionless groups listed in Table S5, eqn (1) may now be rewritten in non-dimensional terms as follows:

$$\frac{\beta}{\tau} = -A \left(\frac{\alpha}{R_p} \right)^2 \pm \left[A^2 \left(\frac{\alpha}{R_p} \right)^4 - B \left(\frac{\alpha}{R_p} \right)^3 - C \left(\frac{\alpha}{R_p} \right) \right]^{1/2} \quad (4)$$

Where,

$$A = \frac{2\mu_p}{\rho_p} \left(\frac{1 + \mu_r}{1 + \rho_r} \right), \quad B = \frac{\sigma}{\rho_p (\rho_r + 1)}, \quad C = \left(\frac{\rho_r - 1}{\rho_r + 1} \right) g \quad (5)$$

Table S5: Non-dimensional numbers used in the study.

Dimensionless Group	Mathematical Expression
Ohnesorge number	$Oh_b = \frac{\mu_b}{\sqrt{\rho_b \sigma_{pb} R_p}}$
Reynolds number	$Re_p = \frac{\rho_p V R_p}{\mu_d}$
Bond number	$Bo = \frac{(\rho_b - \rho_r) g R_p^2}{\sigma_{pb}}$
Froude number	$Fr_p = \frac{V}{\sqrt{g R_p}}$
Weber number	$We_p = \frac{\rho_d V^2 R_p}{\sigma_{pb}}$

Continuing further and setting, $\tau = R_p/V$, [†] where V is the characteristic velocity scale, we may recast equation (1) in terms of non dimensional quantities as,

$$\beta = -A' \alpha^2 \pm [A'^2 \alpha^4 - B' \alpha^3 - C' \alpha]^{1/2} \quad (6)$$

Here,

$$A' = \frac{2}{Re_p} \left(\frac{1 + \mu_r}{1 + \rho_r} \right), \quad B' = \frac{1}{We_p (\rho_r + 1)}, \quad C' = \left(\frac{\rho_r - 1}{\rho_r + 1} \right) \frac{1}{Fr_p^2} \quad (7)$$

S2.1. Criterion for jetting - the first criticality

Equation (1) may be used to obtain the condition for the first criticality *i.e.* when jetting is expected or equivalently when it stops. This may be rationalized mathematically by setting the term under the square root of eqn (6) greater than 0 – a case which represents monotonically decaying standing waves, given by, $B' \alpha^3 + C' \alpha < A'^2 \alpha^4$. Recognizing that $Fr_p^2 We_p^{-1} = (\rho_r - 1) Bo^{-1}$, $We_p Re_p^{-2} = Oh_p^2$ and $\alpha \sim \mathcal{O}(100) = K$ (where, K is a constant) we obtain the following criteria for jetting,

$$Oh_b < 2\Gamma \sqrt{\frac{1}{K} + \frac{Bo}{K^3}} \quad \text{where, } \Gamma = \frac{\mu_r}{(1 + \mu_r)} \sqrt{1 + \frac{1}{\rho_r}} \quad (8)$$

Simplifying eqn (8) further yields the result given below.

$$Oh_b < a \left(\frac{\mu_r}{1 + \mu_r} \right) \quad (9)$$

Where, $a = 2\sqrt{\left(\frac{1}{K} + \frac{Bo}{K^3}\right) \left(\frac{1 + \rho_r}{\rho_r}\right)}$ is a constant.

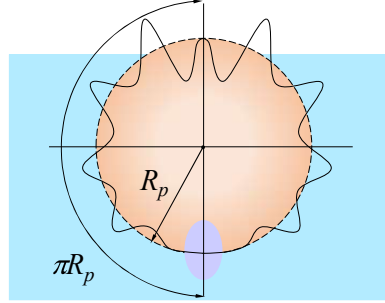
The constant a may be further simplified for cases close to our experimental conditions, $Bo \leq 1.2$ and $\rho_r \approx 1$. and results in a value equal to $\sqrt{8/K}$. In order to determine K we measure the wavelength of the traveling waves in our experiments and compute $K \approx 300$ which when substituted in the expression above results in $a \approx 0.16$.

[†]We may write, τ as the inertial time scale ($= \sqrt{\rho R_p^3 / \sigma}$) or the visco-capillary time scale ($= \mu_p R_p / \sigma_{pb}$), employing the length scale, R_p .

S2.2. Criterion for jetting producing daughter droplets - the second criticality

In this section we describe the scenario when jetting is accompanied by production of daughter droplets. Previous works (11, 12, 32) have established a criterion when jetting produces a daughter droplet and is mathematically expressed by, $\mathcal{D}t < 1$, where, t is the time taken by the traveling wave to reach the apex of the drop as shown in figure S2. The time t may be written as $\pi R_p / v$ ($= \pi R_p k / \omega$) where, v is the wave velocity[†].

(i) Jetting - no droplet generation



(ii) Jetting - droplet generation

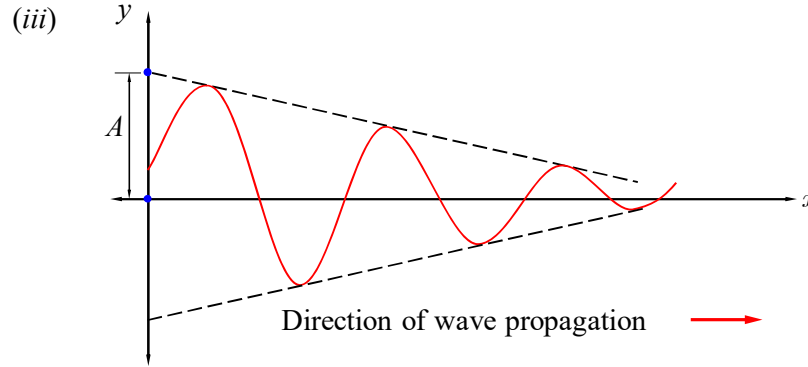
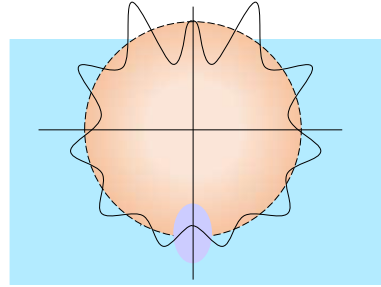


Figure S2: Waves at the parent drop, bulk fluid interface (greatly exaggerated for clarity). (i) Interference of waves at the apex leading to “no jetting” (ii) Interference of waves at the apex leading to “jetting”. Note that the purple shaded region specifically shows this jetting region. (iii) Representation of a traveling wave as transformed from a hemispherical interface to a planar interface showing its attenuation (depicted by decreasing amplitude, A) as it travels.

The above mentioned criterion may be used for our case with suitable corrections as listed below:

1. The wave speed is corrected for its slowing down due to viscosity (of both fluids).
2. Gravity effects are included for the sake of generality.

The above considerations mean we may write $\omega = \sqrt{Bk^3 + Ck - A^2k^4}$ and dissipation, $\mathcal{D} = Ak^2$ which are in their dimensional form and the constants, A, B and C given by eqn (5). This gives us the following criterion for generation of daughter droplets,

$$\frac{A (\pi R_p) k^3}{\sqrt{Bk^3 + Ck - A^2k^4}} < 1 \quad (10)$$

[†]The distance traveled by the traveling wave is taken to be half of the total circumference ($2\pi R_p$) of the two dimensional cross section of the drop. In exact terms, this may differ due to the shape of the drop and the fact that part of its time the wave travels above the flat liquid-air interface and is sandwiched between air and the liquid drop.

To compare this expression with previously obtained results (12) we make the following assumptions. First, we take $\mu_b \gg \mu_d$ and $\rho_b \gg \rho_p$ i.e. $\mu_r^{-1} \ll 1$ and $\rho_r^{-1} \ll 1$. On doing so we obtain, $A = 2\nu_b$. Furthermore in eqn (10) from the denominator we drop the gravity term, C and the term representing the reduction in velocity due to viscous retardation, A^2k^4 . All these simplifications lead to,

$$\frac{A(\pi R_p)k^3}{\sqrt{Bk^3}} < 1 \quad (11)$$

Which reduces to (in non-dimensional terms),

$$2\pi Oh_b \alpha^{3/2} < 1 \quad \text{where,} \quad \alpha = kR_p \quad (12)$$

The condition obtained in eqn (12) matches exactly with that given in works of Blanchett *et al.* (11,12). Substituting the values of A , B and C in eqn (10) in non-dimensional terms we may write,

$$4Oh_b^2 \alpha \left[\frac{\rho_r(1+\mu_r)^2}{\mu_r^2(1+\rho_r)} \right] (\pi^2 \alpha^2 + 1) < 1 + \frac{Bo}{\alpha^2} \quad (13)$$

Substituting for Γ as defined in equation (8) and setting constant, $M = \alpha = \mathcal{O}(1)$ [†] leads to the criterion given below,

$$Oh_b < \Gamma \sqrt{1 + \frac{Bo}{M^2}} \sqrt{\frac{1}{4M(\pi^2 M^2 + 1)}} \quad (14)$$

Noting that constant $M = \mathcal{O}(1)$ like in section S2.1 and further simplifying we get,

$$Oh_b < b \left(\frac{\mu_r}{1 + \mu_r} \right) \quad (15)$$

Here, the constant $b = \frac{1}{2} \sqrt{\left(\frac{1 + \rho_r}{\rho_r} \right) \left(\frac{1}{M} + \frac{Bo}{M^3} \right) \left(\frac{1}{\pi^2 M^2 + 1} \right)} = \frac{a}{2} \sqrt{\frac{1}{\pi^2 M^2 + 1}}$

With simplification as indicated in section S2.1 for Bo and ρ_r we get the value of the constant b as, $\sqrt{\frac{1}{2M(\pi^2 M^2 + 1)}}$. For our test conditions the value of $M \approx 3.5$ which results in $b \approx 0.035$.

S3. Scaling for radius of daughter droplets, R_d

We begin by giving a list of scales which may be useful for further analysis and presented in table S6 below. The absence of any subscript implies the quantities are equally applicable for both, the parent drop (p) and the bulk (b).

S3.1. Scaling for ‘ l ’ and ‘ d ’

To obtain the scaling for l and d we look at the balance of viscous force, $F_v \sim (\mu_b V/R_p)ld$ and capillary force $F_c \sim \sigma_{pb}d$ [†] at the moving front of the cylindrical liquid mass as shown in Figure S3. Noting that $V \sim l/t$ this leads us

[†]The constants K and M are of different order because they correspond to different regimes. For high viscosity ratios, $\mu_r \gg 1$ the instability is pushed to shorter wavelengths and the product $K = \alpha R_p$ is $\mathcal{O}(10)$, a conclusion confirmed by our experiments and previous work (48) which gives typical values of αR_p between 10 – 100. This also explains why higher (bulk) water - glycerol concentrations give daughter droplets of small sizes. With similar considerations one may readily infer that when μ_r is significantly less the instability moves to larger wavelengths and the product $M = \alpha R_p$ is $\mathcal{O}(1)$ giving rise to values of αR_p between 1 – 10.

[†]The curvature term representative of $\vec{\nabla} \cdot \hat{\mathbf{n}} = \frac{1}{R_1} + \frac{1}{R_2}$ scales as d^{-1} since $R_1 \sim d$ and $R_2 \approx \infty$

Table S6: Scaling used in the study.

Regime	τ (s)	V (m/s)	ℓ (m)	Re	Fr	We
Inertial (<i>in</i>)	$\sqrt{\frac{\rho R^3}{\sigma}}$	$\sqrt{\frac{\sigma}{\rho R}}$	R	$\frac{1}{Oh}$	$\frac{\rho_r - 1}{Bo}$	1
Inertio-Visco-capillary (<i>v</i>)	$\frac{\mu^3}{\rho \sigma^2}$	$\frac{\sigma}{\mu}$	$\frac{\mu^2}{\rho \sigma}$	$\frac{1}{Oh^2}$	$\frac{\rho_r - 1}{Oh^2 Bo}$	$\frac{1}{Oh^2}$
Visco-capillary (<i>vc</i>)	$\frac{\mu R}{\sigma}$	$\frac{\sigma}{\mu}$	R	$\frac{1}{Oh^2}$	$\frac{\sqrt{\rho_r - 1}}{Oh \sqrt{Bo}}$	$\frac{1}{Oh^2}$

to the following result,

$$\left(\frac{l}{R_p}\right)^2 \sim \frac{\tau_{in}}{\tau_{vc}} \sqrt{\frac{1}{\rho_r}} \quad (16)$$

In the above, subscript, ‘*in*’ stands for the inertial time scale and ‘*vc*’ for visco-capillary time scale as given in table S6. In eqn (16) t in $V \sim l/t$ is taken as the inertial time scale and the flow inside the cylindrical liquid mass is considered inviscid.

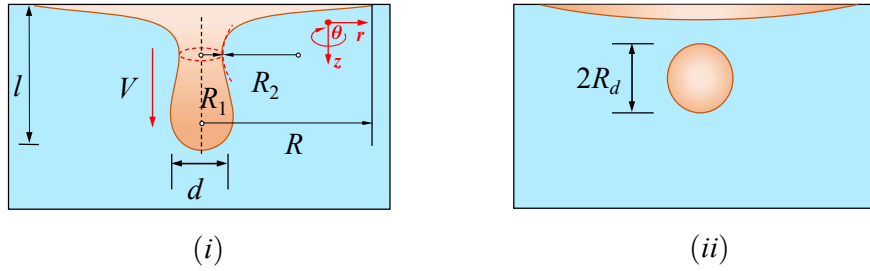


Figure S3: (i) Drop before pinch off at maximum elongation (ii) Daughter droplet (diameter, $D_d = 2R_d$) after pinch off as depicted in Fig 3a of the main manuscript.

Furthermore using the relation, $(l^2/R_p^2) = (l^2/l_v^2) Oh_b^4$ and recognizing that for the test liquids chosen, $\rho_r \sim \mathcal{O}(1)$ we obtain the scaling for ‘ l ’ as,

$$\frac{l}{l_v} \sim Oh_b^{-5/2} \quad (17)$$

Following (35,49) we obtain the scaling for d . To begin with we consider the flow (given by, $\vec{u} = -\vec{\nabla}\phi$) inside the fluid to be inviscid thus it may be described by the Laplace equation, $\nabla^2\phi = 0$ which in cylindrical coordinates (r, θ, z) is written as,

$$\nabla^2\phi = \frac{1}{r} \frac{\partial\phi}{\partial r} \left(r \frac{\partial\phi}{\partial r} \right) + \frac{1}{r^2} \frac{\partial^2\phi}{\partial\theta^2} + \frac{\partial^2\phi}{\partial z^2} \quad (18)$$

Dropping the θ term in equation (18) owing to axisymmetry of the flow. The remaining terms in eqn (18) therefore need to be of the same order in order for the equation to hold. This yields $r \sim z$ which translates to $l \sim d$ and hence the scaling for l and d is the same, a fact confirmed by experimental data which show an exponent of 2.23 and 2.25 for l and d respectively as shown in Fig. S4. Hence we may write the scaling for d as,

$$\frac{d}{l_v} \sim Oh_b^{-5/2} \quad (19)$$

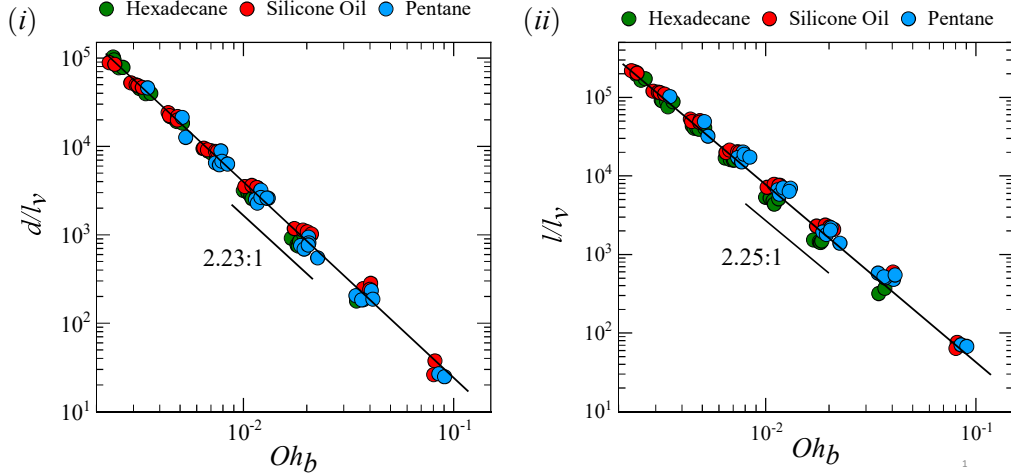


Figure S4: (i) Scaling of l with Oh_b (ii) Scaling of d with Oh_b .

Pursuant of our eventual objective of obtaining the scaling for D_d which is non-dimensionalised by the viscous length scale l_v we substitute eqn (17) and eqn (19) in the mass conservation before and after pinch off (see main paper, Fig. S3)

$$R_d/l_v \sim Oh_b^{-5/2} \quad (20)$$

The scaling exponent of -2.5 obtained in equation eqn (20) is within 7% of the experimentally obtained value of 2.34. Finally, we present raw data corresponding to the daughter droplet sizes plotted in Fig 3 of the main manuscript.

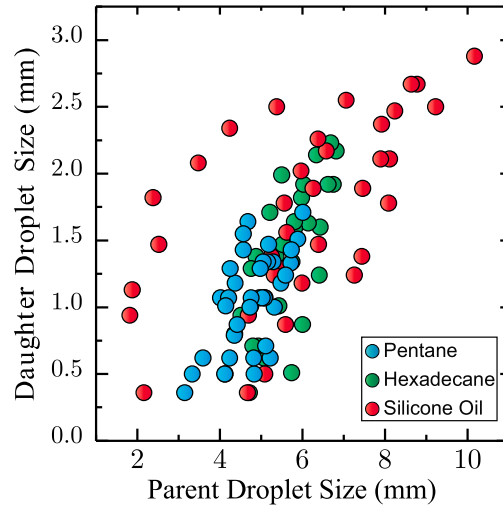


Figure S5: Daughter droplet size against parent drop size for pentane (●), hexadecane(●) and silicone oil (●).

S4. Synthesis of pickered drops

The cascade of bursting events can be arrested to produce armored or pickered drops using micron sized particles. To this end, we use hydrophilic Bentonite (CAS: 1302-78-9) clay particles in the drop to synthesize pickered drops. The surface morphology of the clay particles is shown in Figure S6 as viewed under a scanning electron microscope (SEM). The clay particles are dispersed in the oil drop at varying concentrations, ϕ (0.5% w/w to 6% w/w) to control the number of bursting events and consequently the size of the pickered droplets. It is observed that upon introduction of the drop into the bulk fluid, the clay particles migrate to the interface of the drop and bulk liquid due to hydrophilicity.

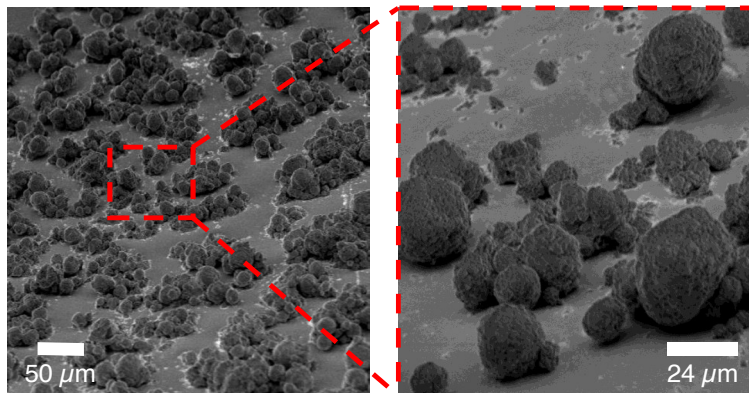


Figure S6: SEM of Bentonite particles.

Following an event of bursting resulting in the generation of a daughter droplet, the concentration of particles at the drop-bulk interface increases due to reduction in surface area as seen in Figure S7 (a) -(c). Simultaneously, a small volume of particles diffuse into the bulk with the emergence of the oil on the surface of the bulk. Depending on

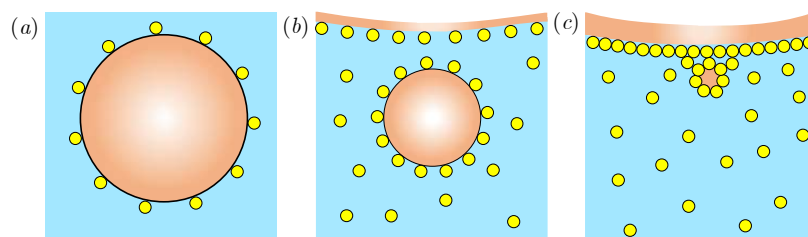


Figure S7: (a) First bursting event (b) Second bursting event (c) Final stable as a pickered drop.

the particle concentration in the parent drop, the surface coverage of the particles at the interface eventually reaches a critical limit, arresting any further bursting events. At this critical limit, the particles are found to self-assemble at the interface to form a shell on the surface of the drop. As described in the main text, the number of bursting events, and eventually the size of the armored drop can be controlled by varying the initial particle concentration in the parent drop.

To verify the adsorption and self assembly of the particles at surface of the oil drop, we introduce a small volume of particle laden oil into a pool of water using an inverted needle. The oil is left attached to the needle for a period of 45 mins before it is retracted back into the syringe. Due to the strong adsorption of the particles at the interface, the retracting oil drop shows a crumpling effect, confirming the formation of a shell at critical surface coverage. Figure S8 shows the morphology of the retracting drop at different time instances. To obtain further proof of the adsorption, we performed Confocal Laser Scanning Microscopy (CLSM) on the drop after one event of bursting. The clay particles were stained using Rhodamine-B (red, laser emission at 610 nm), the bulk liquid was labeled with Fluorescein (green, laser emission at 525 nm), while the oil drop was left unstained. The Rhodamine-B particles were stained by first mixing 10 gm of clay particles in 600 ml of water using a sonicator. Then 250 mg of Rodamine-B was mixed into the solution and mixed again in the sonicator for 30 mins. The powder was allowed to settle to the bottom of the container and collected by draining the excess liquid. The stained particles were washed 3 times using ethanol and a 50:50 mixture of water and NaCl before being vacuum dried at room temperature. Finally the particles were ground using a pestle and mortar before being used. Figure 4b in the main text shows the daughter drop captured under CLSM. It is confirmed through the ring of particles in Figure 4b that the particles indeed adsorb at the interface and form a shell, leading to the arrest of the daughter droplet generation cascade.

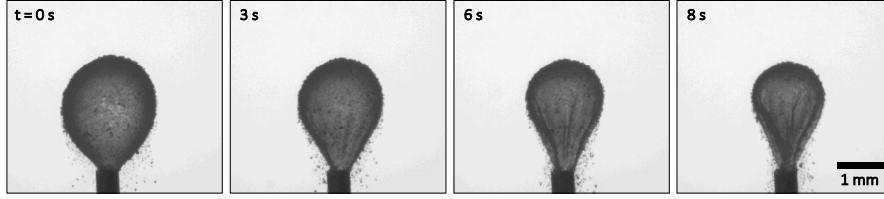


Figure S8: Time instances during retraction and crumpling of a Hexadecane drop with 5% w/w particle concentration. The adsorption of the particles at the interface causes the formation of a membrane at the interface of the oil drop and the bulk liquid.

S5. Partial Coalescence: Daughter droplet cascade

For the case that partial coalescence occurs and complete merger with the bulk proceeds in stages the natural question that arises is – how many bursting events take place before complete coalescence. In this section we shall predict this number using the analysis presented in the previous sections. The discussion is divided into two subsections, (i) First, we predict the number of cascade events (ii) Second, we used theory of limited coalescence to predict arrest of cascade of daughter droplet generation events.

S5.1. Number of daughter droplet generation events, N_e before complete coalescence

Using the analyses derived in the preceding section we can use the relation derived in eqn (15) to predict the number of times (N_e) a parent drop will cascade before completely coalescing with the bulk. If we look closely at the expression for the bulk Ohnesorge number, Oh_b we see that among the factors that can increase its value is R_p , which is the characteristic radius of the impacting drop. During the cascade of the daughter droplet generation events after impact they diminish in size and as a consequence lead to an increase in Oh_b . When the Oh_b increases to the point that it exceeds the values set by eqn (21) the cascade terminates. Moreover, the droplet cascade is seen to decrease the size of the parent drop linearly such that the before the cessation of cascade the final droplet radius, R_N is R_p/N_e . Mathematically, we may write these statements as follows,

$$\sqrt{N_e} Oh_b = b \left(\frac{\mu_r}{1 + \mu_r} \right) \quad (21)$$

Rearranging the terms in equation (21) the obtain the expression for N_e as,

$$N_e = \left[\frac{b\mu_r}{Oh_b(1 + \mu_r)} \right]^2 \quad (22)$$

S5.2. Arrest of partial coalescence with clay particles, N_e as function of φ

The preceding discussion (see section S2.2) have outlined conditions when droplet will be produced on jetting. Upon introduction of hydrophilic particles (weight %, φ) as mentioned in the preceding section the oil/water interface is packed with these particles. For surface coverage, S of about 90%, and $R_p \sim \varphi^{-1}$ we may rewrite eqn (22) as $N_e \propto \varphi^{-1}$ (50). This accurately predicts the variation shown in **Fig. 4(b)** of the main text.

S6. Supplementary Movies

Supplementary Movie 1: Movie S1.mov

Drop bursting events in different bulk liquids.

Burst 0% glycerol : Rupture of the thin liquid film of the bulk liquid when a Hexadecane drop is gently impacted onto the air-liquid interface from bottom. The strong influence of capillary waves in the generation of a daughter droplet can be observed due to the relatively low viscosity of the bulk liquid (0% glycerol).

Burst 70% glycerol : The bursting of a Hexadecane drop in a bulk liquid containing 70% glycerol and 30% water consists of a weak jet downwards. It is evident that the capillary waves are significantly damped by the viscosity of

the bulk fluid and no daughter droplet is generated.

Burst 80% glycerol : The emergence of a Hexadecane drop in a liquid composed of 80% glycerol and 20% water shows minimal effect of the capillary waves in deforming the drop during bursting.

Supplementary Movie 2: Movie S2.mov

Rupture of bulk liquid film.

The oblique and top views of the rupture of the thin film of bulk liquid (water) when a drop of Hexadecane is introduced at the interface from below. Both views show the generation of a daughter droplet below the surface of the water. The top view shows the rupture and retraction of the bulk liquid film preceding the spreading of the oil drop.

Supplementary Movie 3: Movie S3.mov

Cascade of daughter droplet generation events.

The complete emergence of the volume of oil on top of the bulk liquid is an iterative process consisting of multiple bursting events. The bursting events produce subsequent generations of daughter droplets until the droplet reaches a critical Oh_b . Video shows the cascade of daughter droplet generation events leading up to complete emergence of a Hexadecane drop.

Supplementary Movie 4: Movie S4.mov

Effect of particle concentration on arrest of daughter droplet generation cascade.

Particle laden oil drops introduced in the bulk arrest the daughter droplet generation cascade and stabilize the resultant pickered drops. A Hexadecane drop with a particle concentration (ϕ) of 1% w/w undergoes 3 bursting events before a stable pickered drop is achieved. With higher particle concentration, a stable pickered drop is achieved in fewer bursting events ($\phi = 3%$ w/w, 2 bursting events; $\phi = 6%$ w/w, 1 bursting event). The increase in particle concentration also produces larger pickered drops owing to earlier arrest of the cascade.

Supplementary Movie 5: Movie S5.mov

Outcomes of bursting of compound drops.

Compound drops comprising of water and oil components are introduced at the air-water interface. Schematic shows two limiting cases of w/o compound drops with different volume fractions (water : oil 0.1%, 98%).

(a) The increase in the volume fraction of water in the compound drop from 0.1% to 3.4% after bursting.

(b) The fragmentation of oil film under the surface of water in the case of high volume fraction of water (98%). The oil film ruptures, leading to fragmentation of the retracting film induced by the Rayleigh–Plateau instability. The fragmentation generates polydispersed oil drops under the surface of the water.

Supplementary Movie 6: Movie S6.mov

Drop impact from above: entrainment and bursting.

The impact of a Hexadecane drop with velocity 1 m/s onto a pool of water covered by a thin film of Hexadecane from above. The impact entrains oil drops under the surface of the water which subsequently burst and generate daughter droplets. The entrainment of the oil is accompanied by the trapping of ambient air inside the entrained oil drop.